

Perceptual Color Correction Through Variational Techniques

Marcelo Bertalmío, Vicent Caselles, *Associate Member, IEEE*, Edoardo Provenzi, and Alessandro Rizzi

Abstract—In this paper, we present a discussion about perceptual-based color correction of digital images in the framework of variational techniques. We propose a novel image functional whose minimization produces a perceptually inspired color enhanced version of the original. The variational formulation permits a more flexible local control of contrast adjustment and attachment to data. We show that a numerical implementation of the gradient descent technique applied to this energy functional coincides with the equation of automatic color enhancement (ACE), a particular perceptual-based model of color enhancement. Moreover, we prove that a numerical approximation of the Euler–Lagrange equation reduces the computational complexity of ACE from $\mathcal{O}(N^2)$ to $\mathcal{O}(N \log N)$, where N is the total number of pixels in the image.

Index Terms—Automatic color enhancement (ACE), color appearance, color perception, histogram equalization, variational techniques.

I. INTRODUCTION

THE use of ordinary and partial differential equations (PDEs) and variational techniques for image processing became a major research topic in recent years (see [1]–[4] and references therein).

One of the reasons for such interest is the fact that functional methods allow us to deal with several problems of image processing at the same time, thanks to the natural possibility of combining different types of algorithms in the framework of PDEs or variational techniques. Moreover, making explicit the energy functional underlying a given algorithm may reveal relevant properties related to important visual information carried by an image, which may be not very easy to point out only with the analysis of the basic (discrete) formulae. Finally, the functional procedures can be implemented with efficient numerical methods that give highly accurate results.

Manuscript received June 13, 2006; revised November 14, 2006. M. Bertalmío and V. Caselles were supported in part by the PNPGC project, reference BFM2003-02125, and in part by the IP-RACINE Project. M. Bertalmío was supported by the Ramón y Cajal Program. V. Caselles was supported in part by the Departament d'Universitats, Recerca i Societat de la Informació de la Generalitat de Catalunya. E. Provenzi and A. Rizzi were supported by the PRIN-MIUR research project, 2005115173-002. The associate editor coordinating the review of this manuscript and approving it for publication was Dr. Luca Lucchese.

M. Bertalmío and V. Caselles are with the Departament de Tecnologia, Universitat Pompeu Fabra, 08003 Barcelona, Spain (e-mail: marcelo.bertalmio@upf.edu; vicent.caselles@upf.edu).

E. Provenzi and A. Rizzi are with the Dipartimento di Tecnologia dell'Informazione, Università di Milano, Crema (CR) 26013, Italy (e-mail: provenzi@dti.unimi.it; rizzi@dti.unimi.it).

Color versions of one or more of the figures in this paper are available online at <http://ieeexplore.ieee.org>.

Digital Object Identifier 10.1109/TIP.2007.891777

In [1], it has been proven that variational techniques are particularly suitable to perform histogram equalization and matching. However, the contrast modifications induced by the minimization of the energy functional considered in the aforementioned paper did not take into account the spatial, local and nonlinear features of the Human Visual System (HVS), which are instead the guiding lines of perception models.

These characteristics are implemented in a recent perceptual-inspired color correction algorithm: automatic color enhancement (ACE) [5], [6], whose equations, though written in a discrete form, show a structure analogous to the one appearing in [1]. In order to explore these similarities, we have been naturally lead to build up a variational formulation of ACE.

The contribution of this paper is manifold. First, we take into account the ACE equation in discrete terms and we show that it can be obtained as the gradient descent of a certain energy functional. On one side, by studying generalizations of the functional associated to ACE, we may understand which variational methods are suitable for color enhancement based on some properties of the HVS. On the other side, the particular form of the ACE energy functional reveals explicit features of the model which are intrinsic in the discrete framework.

Moreover, this formulation allows an alternative way to investigate the local and global behavior of ACE and a different way to control its effects. Indeed, in the variational setting, ACE can be easily combined with local attachment to data in order to avoid over-enhancement and, eventually, to add a regularization mechanism.

Finally, the combination of the gradient descent technique for the minimization of the ACE functional with a numerical approximation of the related Euler–Lagrange equation allows us to rewrite the model in such a way that its computational complexity decreases from the original $\mathcal{O}(N^2)$ to $\mathcal{O}(N \log(N))$, being N the number of pixels in the image being processed. In practice, this means that high quality perceptual-based color corrected versions of high resolution images may be obtained in a matter of seconds, instead of tens of minutes, with a regular PC (P4, 3 GHz).

We stress that our aim is not to propose an exact model of human vision, but to use fundamental mechanisms of visual perception to develop a framework able to enhance and correct color information with the implementation of a set of human vision characteristics: spatial color recomputation, visual information maximization, global and local filtering effects, and data-driven filtering behavior. The proposed framework could be taken as a starting point for the development of a more biologically consistent model, but its connection with biological basis requires further investigation.

This paper is organized as follows. In Section II, we review the basic facts about global histogram equalization via variational techniques. Section III contains a brief review of the basic ACE formulation. In Section IV, we present a general discussion about local contrast enhancement in the variational framework, pointing out its flexibility. In Section V, the variational formulation of ACE is explored. Section VI deals with the numerical methods to implement the functional description of ACE and the consequent complexity reduction of the related algorithm. Section VII compares the parameters of basic ACE with its variational version. In Section VIII, we present and discuss the results obtained with our proposed approach for several applications and different sorts of images. We end in Section IX with conclusions and perspectives. For the sake of readability, we collected all the proofs of the theorems in the Appendix.

II. HISTOGRAM EQUALIZATION VIA VARIATIONAL TECHNIQUES

In this section, we review how the uniform histogram equalization of an image can be described within the framework of variational principles. First of all, let us focus on the notation that will be used in the paper. Given any RGB image, we indicate with $\mathfrak{J} = [0, W] \times [0, H] \subset \mathbb{R}^2$ its spatial domain. With $x = (x_1, x_2)$ and $y = (y_1, y_2)$, we denote the coordinates of two arbitrary pixels in \mathfrak{J} . For technical reasons, it is worthwhile to normalize the dynamic range of the image in the unit real interval $[0,1]$, so the image function is $\vec{I} : \mathfrak{J} \rightarrow [0,1]^3$, $\vec{I}(x) = (I_R(x), I_G(x), I_B(x))$, where $I_c(x)$ is the intensity level of the pixel $x \in \mathfrak{J}$ in the chromatic channel $c \in \{R, G, B\}$. Since the aim of this paper is to combine variational techniques and color perception algorithms, and since these algorithms perform their computations separately on the scalar components of the image function \vec{I} , we will only deal with a generic scalar image I which will represent any chromatic channel.

This is motivated by the fact that almost every modern perceptual-based color correction algorithm follows the so-called “first postulate of the Retinex theory” [6], which, quoting [7], can be stated as follows: “there are three *independent* lightness-determining mechanisms (one for long, middle and short waves) each operative with less than a millisecond exposure and each served by its own retinal pigment” (for the series of experiments that lead to this postulate see, e.g., [8]).

Now, in [1], it has been proposed an evolution equation whose steady state corresponds to the histogram equalization of the initial image. This formulation permits some flexibility to design local contrast enhancement principles and can be extended to color images. Let us briefly recall the basic facts about [1].

Let $\psi : [0, 1] \rightarrow \mathbb{R}$ be a differentiable function defined in the codomain of the image function. Consider the functional

$$E(I) = \int_{\mathfrak{J}} \psi(I(x)) dx - \frac{1}{WH} \int_{\mathfrak{J}} \int_{\mathfrak{J}} |I(x) - I(y)| dx dy. \quad (1)$$

Later on, we will give an interpretation of $E(I)$. Let us state that the first variation of the energy $E(I)$ is given by

$$\delta E(I) = \psi'(I(x)) + 2 - \frac{4}{WH} \int_{\mathfrak{J}} \text{sign}^+(I(x) - I(y)) dy \quad (2)$$

where

$$\text{sign}^+(t) = \begin{cases} 1, & t > 0 \\ \frac{1}{2}, & t = 0 \\ 0, & t < 0 \end{cases}.$$

The formal proof of this statement can be found in Appendix A.

To simplify the notation, let us write $I(x) \equiv \lambda$. Then we define

$$H_I(\lambda) \equiv \frac{1}{WH} \int_{\mathfrak{J}} \text{sign}^+(\lambda - I(y)) dy \quad \lambda \in [0, 1]. \quad (3)$$

If λ is such that $\text{Area}(\{y \in \mathfrak{J} : I(y) = \lambda\}) = 0$ for every $\lambda \in [0, 1]$, then $H_I(\lambda) = \lambda$ represents the cumulative histogram of I . In particular, if $H_I(\lambda) = \lambda$ for any $\lambda \in [0, 1]$, we say that I has a uniform histogram. On the other hand, it is well known that the pixel transformation $\lambda \mapsto (1/WH) \int_{\mathfrak{J}} \text{sign}^+(\lambda - I(y)) dy$ leads to an image with a uniformly equalized histogram (see, for instance, [9]).

With this notation, we may write (2) as

$$\delta E(I) = \psi'(\lambda) + 2 - 4H_I(\lambda). \quad (4)$$

If I is a stationary image, i.e., if $\delta E(I) = 0$, then

$$H_I(\lambda) = \frac{\psi'(\lambda) + 2}{4}. \quad (5)$$

Hence, if we choose

$$\psi'(\lambda) = 4\lambda - 2 \quad (6)$$

i.e., if $\psi(\lambda) = 2\lambda^2 - 2\lambda + K$, where K is an arbitrary constant, then $H_I(\lambda) = \lambda$, for every $\lambda \in [0, 1]$, and this corresponds to the uniform histogram equalization. Choosing $K = 1/2$, we get

$$\psi(\lambda) = 2 \left(\lambda - \frac{1}{2} \right)^2. \quad (7)$$

So, writing again $I(x)$ instead of λ , we find that the functional whose minimization leads to a constant histogram equalization¹ is

$$E(I) = 2 \int_{\mathfrak{J}} \left(I(x) - \frac{1}{2} \right)^2 dx - \frac{1}{WH} \int_{\mathfrak{J}} \int_{\mathfrak{J}} |I(x) - I(y)| dx dy. \quad (10)$$

If we define the average contrast of the image I as the quantity

$$C(I) \equiv \frac{1}{WH} \int_{\mathfrak{J}} \int_{\mathfrak{J}} |I(x) - I(y)| dx dy \quad (11)$$

¹There are other variational principles whose minima permit to specify the histogram of the image, but they do not offer the advantages of (1) in view of later generalizations. Let $h : [0, 1] \rightarrow [0, 1]$ be a distribution function. The most simple one is given by

$$E_h(I) = \int_{\mathfrak{J}} (H_I(I(x)) - h(I(x)))^2 dx. \quad (8)$$

A formal computation (justifiable under certain hypothesis) proves that

$$\delta E_h(I) = -2(H_I(I(x)) - h(I(x))). \quad (9)$$

Since we do not need this in this paper, we shall not reproduce the details here.



Fig. 1. (Left) Original image, after (right) global histogram equalization. Courtesy of P. Greenspun.

then we can see that minimizing the energy $E(I)$ for all images $I : \mathcal{I} \rightarrow [0, 1]$ amounts to maximizing the average contrast of the image while minimizing its deviation with respect to its theoretical mean $1/2$. This is an interesting “view from above” on the problem of color enhancement, and we will generalize it in Section IV.

If we denote with I_0 the initial image, we have, under some mild assumptions (see [1]), the gradient descent of the energy (10), i.e., the problem

$$\begin{cases} \frac{\partial I}{\partial t} = -\delta E(I) \\ I(0) = I_0 \end{cases} \quad (12)$$

has a unique solution that can be found explicitly. The reason for the use of an evolution equation instead of the direct computation of the steady state is that (12) transports gradually the histogram of the image I_0 toward a uniform one, and it allows a user to stop whenever the image looks as desired, being the case that often the final result, where the histogram is flat, looks unrealistic, or washed out, or too saturated.

As disadvantages of this formulation we should mention two. First, the evolution preserves the ordering of the level lines (see Section V-B) and it does not take into account locality in space, so it does not comply with basic human visual perception properties. Second, the computational complexity is rather high: $O(N^2)$, where N is the total number of pixels in the image.²

In Fig. 1 (left), we show a classical example of backlight image for which the global histogram equalization technique gives an unsatisfactory result, Fig. 1 (right).

In the following section, we will look at the problem of color enhancement from a completely different perspective, that of perceptual-based algorithms.

III. ACE BASIC FORMULATION

Starting from the revolutionary Retinex model of color perception by Land and McCann [15], several further models have been developed to reproduce and analyze how the HVS perceives colors [10]. The aim of all color perception algorithms is to map, for every fixed chromatic channel, the colorimetric intensity $I(x)$ of a pixel x into the corresponding perceptual quantity, called *lightness* after Land and McCann and indicated with $L(x)$ in this present paper. The recombination of the lightness in all channels gives the triplet that estimates the color appearance of the pixel x . We note that, since the goal of the model

²On a P4, 3-GHz PC, it would take up to one hour to process a high-resolution image.

that we present here is image enhancement, the lightness may correspond qualitatively but not necessarily quantitatively to the perceptual correlate.

There are three paramount important characteristics of the HVS that every perceptual-inspired model should implement: the first is *locality* of color perception, i.e., the fact that the HVS is strongly influenced by the global and local context in which an observed scene lies [12]–[14]; the second is the *spatial nature* of the color perception, meaning that the actual sensation image induced by the HVS follows from a comparison of local information coming from different image areas [16]; finally, the HVS exhibits *nonlinear* responses both to global and local variations of the stimuli coming from an observed scene [17].

In this paper, we choose to analyze ACE [5], [6] for its similarities with contrast enhancement techniques. Since ACE was originally developed for digital images, we shall restrict us to this case in this section. We shall use kernels to localize quantities expressed by sums over the image, so let us precise our image domain. Given a digital image I initially defined in $\{1, \dots, W\} \times \{1, \dots, H\}$, we extend it as an even function with respect to the two variables in the domain $\{-W + 1, \dots, W\} \times \{-H + 1, \dots, H\}$ and then by periodicity to $\mathbb{Z} \times \mathbb{Z}$ with fundamental period $\{-W + 1, \dots, W\} \times \{-H + 1, \dots, H\}$. For simplicity, we denote the extended image again by I . With this, we may consider the domain of I as the periodic sampling lattice; that is, $\mathbb{T}_d := (\mathbb{Z} \times \mathbb{Z}) / (2W\mathbb{Z} \times 2H\mathbb{Z})$.³

To show how ACE works, we will present the formulae that characterize this filter and then discuss their meaning. In the ACE framework, $x \in \mathbb{T}_d$ represents a fixed pixel, called *target*, whose intensity $I(x)$ must be recomputed into the lightness $L(x)$, while y denotes a generic pixel in the rest of the image. Given a real constant $\alpha > 1$, we build up the following odd function: $s_\alpha : [-1, 1] \rightarrow [-1, 1]$

$$s_\alpha(r) = \begin{cases} -1, & \text{if } -1 \leq r \leq -\frac{1}{\alpha} \\ \alpha r, & \text{if } -\frac{1}{\alpha} < r < \frac{1}{\alpha} \\ +1, & \text{if } \frac{1}{\alpha} \leq r \leq 1 \end{cases} \quad (13)$$

α and s_α are called, respectively, slope and slope function. We will be interested in the case when $r = I(x) - I(y)$, where x is a fixed image pixel and y varies across the image.

³This notation means that we have identified any two points $x = (x_1, x_2)$ and $y = (y_1, y_2)$ in $\mathbb{Z} \times \mathbb{Z}$ if $x_1 - y_1 \in 2W\mathbb{Z}$ and $x_2 - y_2 \in 2H\mathbb{Z}$. We denote this equivalence relation by \equiv . The distance between any two points $x, y \in \mathbb{T}_d$, denoted by $\|x - y\|_{\mathbb{T}_d}$, is computed as $\min\{|\bar{x} - \bar{y}| : \bar{x} \equiv x, \bar{y} \equiv y\}$, where $|v| = \sqrt{v_1^2 + v_2^2}$, $v = (v_1, v_2)$. From now on, we shall assume that our images have this symmetry properties and are defined in \mathbb{T}_d .

It is also important to introduce a symmetric weight function $\omega : \mathbb{T}_d \times \mathbb{T}_d \rightarrow \mathbb{R}^+$, i.e., $\omega(x, y) = \omega(y, x)$ for every $x, y \in \mathbb{T}_d$, where $\omega(x, y)$ represents the weight of mutual chromatic influence between the pixels x and y .

The lightness computation of the target pixel x is performed by ACE in two steps. First of all, it computes the *chromatic spatial adjustment*, i.e.,

$$R(x) = \frac{\sum_{y \in \mathbb{T}_d} \omega(x, y) s_\alpha(I(x) - I(y))}{\sum_{y \in \mathbb{T}_d} \omega(x, y)}. \quad (14)$$

Then it performs the *dynamic tone reproduction scaling* of $R(x)$ into the normalized dynamic range, computing the target pixel x as

$$L(x) = \frac{1}{2} + \frac{R(x)}{2M} \quad (15)$$

where $M = \max_{x \in \mathbb{T}_d} \{R(x)\}$.

We start the analysis of the previous formulae noticing that ACE implements the spatial nature of color computation using differences between the intensities of the target pixel and the other image pixels. The reason for the use of differences in ACE is that they are the most natural operations to jointly implement the differential nature of spatial comparisons and the “gray world” (GW) principle. This can be easily understood considering the toy model of an image with only two pixels x and y . If we define $D_{xy} = I(x) - I(y)$, then $D_{yx} = -D_{xy}$, so their average is 0. The null value can then be mapped to the middle gray with the simple translation by the term $1/2$, as done in formula (15). The same results can be obtained considering an image of any size and using an odd function of $I(x) - I(y)$, because the average value of any odd function is 0. This is why the oddness of s_α is an essential feature for ACE.

It is important to notice that the slope function induces a nonlinear behavior. In fact, in the region $-(1/\alpha) < I(x) - I(y) < (1/\alpha)$, i.e., for relatively small intensity differences, s_α increases the contrast, mapping $I(x) - I(y)$ into $\alpha(I(x) - I(y))$ with $\alpha > 1$. Conversely, for relatively big intensity differences, s_α saturates.

Finally, in ACE, locality is achieved thanks to the weight function ω , which must be a monotonically decreasing function of $\|x - y\|_{\mathbb{T}_d}$ according to experiments on color perception [12]–[14]. The tuning performed in [5] showed that the weight function that corresponds to good performances of the algorithm is $\omega(x, y) = 1/\|x - y\|_{\mathbb{T}_d}$, $y \in \mathbb{T}_d \setminus \{x\}$, i.e., the inverse of the Euclidean distance between pixels. The value $\omega(x, x)$ is undefined, and the sums above are only extended to $\mathbb{T}_d \setminus \{x\}$. By defining $\omega(x, x) = 0$, we can write the sums in all \mathbb{T}_d . The division by $\sum_{y \in \mathbb{T}_d} \omega(x, y)$ is needed to correctly normalize the computation.

Notice that there surely exists, at least, one pixel x , such that $R(x) = M$. After the dynamic mapping, its value will become 1. For this reason, ACE, to maximize the output dynamic range, also implements, besides the GW assumption, even the so-called “white patch” (WP) assumption, which states that there is at least one white object in an observed scene.



Fig. 2. ACE filtered version of the image in Fig. 1. Courtesy of P. Greenspun.

As Retinex, ACE shows a strong ability to remove color cast from images [5], [6]. Moreover, it can deal both with under and over-exposed images, since it does not always increase the pixel intensity, as opposed to the Retinex algorithm (the mathematical proof of this fact can be found in [19]). Thanks to the presence of the slope function, ACE increases the percentage of used chromatic dynamics and the flatness of its histogram. Global and local contrast can vary independently, i.e., one may increase and the other decrease. As for disadvantages of ACE, we will mention the following. There are several open questions regarding the theoretical foundations of the algorithm: Is it idempotent? If it is not, does it converge when iterated? How does it modify image contrast and variance? From a practical point of view, the major drawback of ACE is its high computational cost [5], [6]: $O(N^2)$ where N is the total number of pixels in the image.

In Fig. 2, we can see the same original picture appearing in Fig. 1 (left) filtered with ACE. Notice that local filtering allows us to adjust contrast in the dark areas in a more balanced and visually pleasing way than global histogram equalization technique.

IV. LOCAL CONTRAST ENHANCEMENT VIA VARIATIONAL TECHNIQUES

We shall extend in two directions the variational principle reviewed in Section II, first considering more general contrast measures and then interpreting them in a local way. As in the last section, since images are defined in a finite domain, typically a rectangle, and since we shall use kernels to localize quantities expressed by integrals, let us precise our integration domain. Given any image $I : \mathcal{J} \rightarrow [0, 1]$, we extend it as an even function on $\mathcal{J}^e := [-W, W] \times [-H, H]$, i.e., we replicate the image specularly in all directions, and then we extend it by periodicity to \mathbb{R}^2 with fundamental period \mathcal{J}^e . With this, we may consider the domain of \mathcal{J}^e as a torus, that is as $\mathbb{T} := \mathbb{R}^2 / (2W\mathbb{Z} \times 2H\mathbb{Z})$.⁴ The extension to the torus is only a way to refer to the periodic extension described above.

⁴This notation means that we have identified any two points $x = (x_1, x_2)$ and $y = (y_1, y_2)$ if $x_1 - y_1 \in 2W\mathbb{Z}$ and $x_2 - y_2 \in 2H\mathbb{Z}$. Again, we denote this equivalence relation by \equiv . The distance between any two points $x, y \in \mathbb{T}$, denoted by $\|x - y\|_{\mathbb{T}}$, is computed as the distance on the torus; that is, as $\min\{\|\bar{x} - \bar{y}\| : \bar{x} \equiv x, \bar{y} \equiv y\}$, where $|v| = \sqrt{v_1^2 + v_2^2}$, $v = (v_1, v_2)$. From now on, we shall assume that our images have this symmetry properties and are defined in \mathbb{T} .

Let $\omega, \tilde{\omega} : \mathbb{T} \times \mathbb{T} \rightarrow \mathbb{R}^+$ be two positive symmetric normalized weight functions, i.e., $\omega(x, y) = \omega(y, x)$ for every $x, y \in \mathbb{T}$ and

$$\int_{\mathbb{T}} \omega(x, y) dy = 1 \quad \forall x \in \mathbb{T} \quad (16)$$

and similarly for $\tilde{\omega}$.

Let $J : \mathbb{R} \rightarrow [0, \infty)$ be a convex even function. We define the average local contrast measure of I as

$$C_{\omega, J}(I) := \int \int_{\mathbb{T}^2} \omega(x, y) J(I(x) - I(y)) dx dy \quad (17)$$

and an average quadratic local dispersion measure as

$$D_{\tilde{\omega}}(I) \equiv \int \int_{\mathbb{T}^2} \tilde{\omega}(x, y) \left(I(y) - \bar{I}^{\tilde{\omega}}(x) \right)^2 dx dy \quad (18)$$

where $\bar{I}^{\tilde{\omega}}(x)$ is a local average. There are several possible choices for $\bar{I}^{\tilde{\omega}}(x)$; in this paper, we will examine the following three.

A. Different Choices of $\bar{I}^{\tilde{\omega}}(x)$

1) *Gray World*: The first choice for $\bar{I}^{\tilde{\omega}}(x)$ is the local version of a perceptually based assumption, called ‘‘gray world’’ [11]. This assumption says that the average channel color intensity in every observed scene is perceived as the middle gray. Mathematically, this can be translated into

$$\bar{I}^{\tilde{\omega}}(x) = \frac{1}{2}. \quad (19)$$

Using the notation $D_{\tilde{\omega}, GW}(I)$ for this choice, we have

$$\begin{aligned} D_{\tilde{\omega}, GW}(I) &\equiv \int \int_{\mathbb{T}^2} \tilde{\omega}(x, y) \left(I(y) - \frac{1}{2} \right)^2 dx dy \\ &= \int_{\mathbb{T}} \left(\int_{\mathbb{T}} \tilde{\omega}(x, y) dx \right) \left(I(y) - \frac{1}{2} \right)^2 dy \\ &= \int_{\mathbb{T}} \left(I(y) - \frac{1}{2} \right)^2 dy. \end{aligned}$$

Thus, this implies the global GW assumption.

The GW principle aims at centering the image pixel values in the middle of the available dynamic range. For the purposes of image enhancement, centering locally the signal in the middle of the available dynamic range maximizes contrast and, consequently, visual information.

2) *Attachment to Original Data*: If I_0 is a given (original) image which we want to enhance, the second choice for $\bar{I}^{\tilde{\omega}}(x)$ that we examine is

$$\bar{I}^{\tilde{\omega}}(x) := \int_{\mathbb{T}} \tilde{\omega}(x, y) I_0(y) dy. \quad (20)$$

We denote the dispersion corresponding to this choice as $D_{\tilde{\omega}, I_0}(I)$.

In this case, the dispersion measure amounts to a control of the local variance of the image. As a limit case of this dispersion, we mention, for later use, the situation in which $\tilde{\omega}(x, y) = \delta(x - y)$, to which corresponds a dispersion

$$D_{\delta, I_0}(I) = \int_{\mathbb{T}} (I(x) - I_0(x))^2 dx. \quad (21)$$

3) *Linear Combination of Gray World and Attachment to Original Data*: We consider here dispersions that are linear combinations of the two previous ones, i.e.,

$$D_{\tilde{\omega}}(I) = \beta D_{\tilde{\omega}, GW}(I) + \gamma D_{\tilde{\omega}, I_0}(I) \quad \beta \geq 0, \gamma > 0. \quad (22)$$

Observe that $D_{\tilde{\omega}, I_0}$ contains an attachment to the original data I_0 .

Collecting this dispersion term and $C_{\omega, J}$, we define the functional

$$E_{\tilde{\omega}, \omega}(I) := D_{\tilde{\omega}}(I) - C_{\omega, J}(I). \quad (23)$$

Minimizing the energy (23) amounts to increasing the contrast while controlling the local variance of the resulting image. Since the purpose of the energy minimization is image enhancement, the important target should be increasing the contrast without making noise visible and without introducing contouring effects (neither over-saturation), respecting the visual content of the image. The attachment to data permits to respect visual content and avoids the undesirable effects just mentioned.

B. Euler–Lagrange Equations of the Energy in the General Case (Section IV-A3)

Given an input image I_0 , our purpose will be to perform this minimization

$$\text{Minimize } E_{\tilde{\omega}, \omega}(I). \quad (24)$$

Later on, we will comment on the existence of minima for this functional. Let us first compute its variation.

Using the symmetry of $\omega(x, y)$, the oddness of J' and repeating the computations of Appendix A, we have

Proposition 1: Assume that J is differentiable. Then

$$\delta C_{\omega, J}(I) := 2 \int_{\mathbb{T}} \omega(x, y) J'(I(y) - I(x)) dy. \quad (25)$$

Remark 1: Proposition 1 can be extended for any convex even function J , even if it is not differentiable. This permits us to consider the case $J(r) = |r|$, $r \in \mathbb{R}$ (see Appendix B).

Obviously, the first variation of $D_{\tilde{\omega}, GW}(I)$ is $\delta D_{\tilde{\omega}, GW}(I)(x) = 2(I(x) - (1/2))$. For $D_{\tilde{\omega}, I_0}$ we have the following proposition.

Proposition 2: The first variation of $D_{\tilde{\omega}, I_0}(I)$ is

$$\delta D_{\tilde{\omega}, I_0}(I)(x) := 2I(x) - 2 \int_{\mathbb{T}} \tilde{\omega}(x, y) \bar{I}^{\tilde{\omega}}(y) dy. \quad (26)$$

For the proof of this proposition, see Appendix C.

Corollary 4.1: Assume that J is differentiable. If I is a minimum of $E_{\tilde{\omega},\omega}$, then

$$2\beta \left(I(x) - \frac{1}{2} \right) + 2\gamma \left(I(x) - \int_{\mathbb{T}} \tilde{\omega}(x,y) \tilde{I}^{\tilde{\omega}}(y) dy \right) - 2 \int_{\mathbb{T}} \omega(x,y) J'(I(y) - I(x)) dy = 0. \quad (27)$$

Remark 2: With suitable modifications, this corollary can be also extended for any convex function J , even if it is not differentiable (see Appendix D).

C. On the Existence of Minima of $E_{\tilde{\omega},\omega}$

Let us now discuss the existence of minima for the functional $E_{\tilde{\omega},\omega}$. Indeed, the existence of minima for $E_{\tilde{\omega},\omega}$ can be proved under some additional assumptions including, in particular, the discrete case. For that, we use the notation introduced in Section III, and we write the energies in a discrete framework. Let $I_0, I : \mathbb{T}_d \rightarrow \mathbb{R}^+$ be two images, where I_0 represents the initial data, and $\tilde{\omega}, \omega : \mathbb{T}_d \times \mathbb{T}_d \rightarrow \mathbb{R}^+$ are symmetric functions such that

$$\sum_{y \in \mathbb{T}_d} \omega(x,y) = \sum_{y \in \mathbb{T}_d} \tilde{\omega}(x,y) = 1 \quad \forall x \in \mathbb{T}_d. \quad (28)$$

We consider the discrete functional

$$E_{\tilde{\omega},\omega}^d(I) := D_{\tilde{\omega}}^d(I) - C_{\omega,J}^d(I) \quad (29)$$

where

$$D_{\tilde{\omega}}^d(I) = \beta D_{\tilde{\omega},GW}^d(I) + \gamma D_{\tilde{\omega},I_0}^d(I), \quad \beta \geq 0, \gamma > 0 \quad (30)$$

$$D_{\tilde{\omega},I_0}^d(I) = \sum_{x \in \mathbb{T}_d} \sum_{y \in \mathbb{T}_d} \tilde{\omega}(x,y) \left(I(y) - \tilde{I}^{\tilde{\omega}}(x) \right)^2 \quad (31)$$

$$\tilde{I}^{\tilde{\omega}}(x) = \sum_{y \in \mathbb{T}_d} \tilde{\omega}(x,y) I_0(y)$$

$$D_{\tilde{\omega},GW}^d(I) = \sum_{x \in \mathbb{T}_d} \left(I(x) - \frac{1}{2} \right)^2 \quad (32)$$

and

$$C_{\omega,J}^d(I) = \sum_{x \in \mathbb{T}_d} \sum_{y \in \mathbb{T}_d} \omega(x,y) J(I(x) - I(y)). \quad (33)$$

Propositions 1, 2, and Corollary 4.1 hold (with the same proofs), replacing integrals by sums with respect to indexes in \mathbb{T}_d . Our next Proposition states the existence of minima for $E_{\tilde{\omega},\omega}^d$.

Proposition 3: If the function J satisfies $J(r) \leq C|r|$ for some constant $C > 0$, then the energy $E_{\tilde{\omega},\omega}^d$ has a minimum in the class of images $I : \mathbb{T}_d \rightarrow \mathbb{R}^+$.

The proof of this proposition can be found in Appendix F and holds also if we use $\tilde{I}^{\tilde{\omega}}(x) = 1/2$.

Remark 3: An analogous proposition can be proved in the continuous case if we replace $C_{\omega,J}(I)$ by $C_{\omega,J}(G * I)$; that is, we replace the image I by its regularized version $G * I$ where G is convolution kernel such as a Gaussian, i.e., see Appendix G.

V. ACE VARIATIONAL FORMULATION

In this section, we are going to show that the variational techniques used in Section IV to perform the local contrast enhancement can also be used to derive the ACE local color correction equalization. To realize this connection, which is formulated in the discrete framework, we use the discrete versions of the energies.

First of all, we notice that, if we write

$$A(x) = \left(\sum_{y \in \mathbb{T}_d} \frac{1}{\|x - y\|_{\mathbb{T}_d}} \right)^{-1} \quad (34)$$

then $A(x)$ is a constant A , i.e., $A(x) = A$ for any $x \in \mathbb{T}_d$ and we can incorporate the normalization factor of (14) into the definition of the weights (keeping, for simplicity, the same notation), i.e.,

$$\omega(x,y) = \frac{A}{\|x - y\|_{\mathbb{T}_d}}, \quad x \neq y. \quad (35)$$

With this choice for the weights, formula (14) relative to the ACE spatial chromatic comparison can be rewritten as

$$R_I(x) := \sum_{y \in \mathbb{T}_d} \omega(x,y) s_{\alpha}(I(x) - I(y)). \quad (36)$$

Consequently

$$\text{ACE}(I)(x) := L(x) = \frac{1}{2} + \frac{\sum_{y \in \mathbb{T}_d} \omega(x,y) s_{\alpha}(I(x) - I(y))}{2M} \quad (37)$$

remembering that $M \equiv \max_{x \in \mathbb{T}_d} \{R_I(x)\}$.

Our aim is now to find out a way to transform $I(x)$ into $L(x)$ using the variational techniques presented in Section IV.

To this end, consider the following functional:

$$E(I) = \frac{1}{2} \sum_{x \in \mathbb{T}_d} \left(I(x) - \frac{1}{2} \right)^2 - \frac{1}{4M} \sum_{x \in \mathbb{T}_d} \sum_{y \in \mathbb{T}_d} \omega(x,y) s_{\alpha}(I(x) - I(y)) \quad (38)$$

where S_{α} is such that $S'_{\alpha} = s_{\alpha}$, being s_{α} the ACE slope function and $0 < M \leq 1$ is a constant to be specified later. The coefficients in front of the terms are normalization constants. The function S_{α} is convex and even, given that its derivative is the odd function s_{α} .

If I is a minimum of E , then $\delta E(I) = 0$ and Corollary 4.1 implies that

$$I(x) = \frac{1}{2} + \frac{\sum_{y \in \mathbb{T}_d} \omega(x,y) s_{\alpha}(I(x) - I(y))}{2M} = L(x) \quad (39)$$

and the right-hand side of this formula is precisely the lightness $L(x)$ computed by ACE, i.e., (37). Thus, this formula says that $L(x)$ is a fixed point of ACE.

Remark 4: If we use a gradient descent strategy to minimize the energy $E(I)$ starting from an initial image I_0 , we have to solve

$$\frac{\partial I}{\partial t} = -\delta E(I). \quad (40)$$

Now, if we use an explicit scheme to discretize (40) with respect to parameter t , then we may write

$$\frac{I^{k+1}(x) - I^k(x)}{\Delta t} = \frac{1}{2} - I^k(x) + \frac{R_{I^k}(x)}{2M} \quad (41)$$

where $\Delta t > 0$, $I^k(x) = I(k\Delta t, x)$, $I^0(x) = I_0(x)$ and $R_{I^k}(x) = \sum_{y \in \mathbb{T}_d} \omega(x, y) s_\alpha(I^k(x) - I^k(y))$. We may write (41) as

$$I^{k+1}(x) = (1 - \Delta t)I^k(x) + \Delta t \left(\frac{1}{2} + \frac{R_{I^k}(x)}{2M} \right). \quad (42)$$

On one hand, taking $M := \max_{x \in \mathbb{T}_d} \{R_{I^0}(x)\}$, $\Delta t = 1$ and $k = 0$, we obtain

$$I^1(x) = \text{ACE}(I_0)(x) = L(x). \quad (43)$$

On the other hand, we can also use (42) as a numerical scheme to get to a steady state of ACE. However, we have observed that this steady state is oftentimes affected by over-contrast that make the output visually unpleasing. For that reason, we use the dispersion measure (22), which penalizes the departure from the original image, i.e., we add an *attachment to data* term. For simplicity, in our experiments in Section VIII we use $\tilde{\omega}(x, y) = \delta(x - y)$ so that $\tilde{I}^\omega(x) = \sum_{z \in \mathbb{T}_d} \tilde{\omega}(x, y) I^0(y) = I^0(x)$, and the parameters $\beta = (1/2)$, $\gamma = \lambda/2$, $\lambda > 0$. In this case, the gradient descent equations are

$$\frac{I^{k+1}(x) - I^k(x)}{\Delta t} = \frac{\sum_{y \in \mathbb{T}_d} \omega(x, y) s_\alpha(I^k(x) - I^k(y))}{2M} + \left(\frac{1}{2} - I^k(x) \right) - \lambda (I^k(x) - I^0(x)) \quad (44)$$

which, after some simple manipulations, may be written as

$$I^{k+1}(x) = (1 - (1 + \lambda)\Delta t)I^k(x) + \Delta t \frac{R_{I^k}(x)}{2M} + \Delta t \left(\frac{1}{2} + \lambda I^0(x) \right) \quad (45)$$

where $0 < \Delta t \leq 1/(1 + \lambda)$. We observe that the right-hand side contains a term that penalizes the departure from the original image by compensating in the opposite direction.

A. Comparison Between Uniform Histogram Equalization and ACE in the Variational Framework

It is interesting to compare the two functionals related to the uniform histogram equalization and to the ACE variational formulation. These functionals are, respectively

$$E_{\text{Hist Eq}}(I) = 2 \sum_{x \in \mathbb{T}_d} \left(I(x) - \frac{1}{2} \right)^2 - \frac{1}{WH} \sum_{x \in \mathbb{T}_d} \sum_{y \in \mathbb{T}_d} |I(x) - I(y)| \quad (46)$$

and

$$E_{\text{ACE}}(I) = 2M \sum_{x \in \mathbb{T}_d} \left(I(x) - \frac{1}{2} \right)^2 - \sum_{x \in \mathbb{T}_d} \sum_{y \in \mathbb{T}_d} \omega(x, y) S_\alpha(I(x) - I(y)). \quad (47)$$

It can be seen that the first term in both functionals contains the energy distribution of the image signal around the middle gray. The minimization of this part of the functionals produces global effects on the image.

The second term instead is very different: for the uniform histogram equalization we have a global contrast measure given by the absolute difference between pixel intensities, which is not suitable by a perceptual perspective. Instead, for the ACE variational formulation, we have a rather complicated contrast measure. This measure is more suitable to reproduce perceptual effects thanks to the presence of the slope and weight functions, that introduce, respectively, the nonlinear and local behavior typical of the HVS.

B. Basic Property of the Model: Locality of Perception and Level Lines

According to the basic postulate of Mathematical Morphology [20] an image I is characterized by its upper (or lower) level sets $X_\lambda = \{x : I(x) \geq \lambda\}$ (resp. $X'_\lambda = \{x : I(x) \leq \lambda\}$) for any value of λ . Upper (resp. lower) level sets are formed by the points where the image pixel values are above (resp. below) $\lambda \in \mathbb{R}$. We note that image I can be recovered from its level sets by the reconstruction formula

$$I(x) = \sup\{\lambda : x \in X_\lambda\}.$$

Level lines are usually defined as the boundaries of the level sets [21] and intuitively represent the iso-level lines of the image. We want to discuss the effect on the level sets of our nonlinear local color enhancement algorithm.

For that, from formula (45) we are led to analyze the properties of the operator

$$\mathcal{H}_{\omega, J}(I(x)) := \int_{\mathbb{T}} \omega(x, y) J'(I(x) - I(y)) dy. \quad (48)$$

Let us analyze first the case of global contrast enhancement.

Proposition 4: Let $J : \mathbb{R} \rightarrow [0, \infty)$ be a convex function. If there is no kernel involved, i.e., $\omega(x, y) = 1/\text{Area}(\mathbb{T})$ and we write $\mathcal{H}_J = \mathcal{H}_{\omega, J}$, then

$$(\mathcal{H}_J(I(x)) - \mathcal{H}_J(I(\tilde{x}))) \cdot (I(x) - I(\tilde{x})) \geq 0. \quad (49)$$

Thus, in the scalar case, if $I(x) < I(\tilde{x})$, then $\mathcal{H}_J(I(x)) \leq \mathcal{H}_J(I(\tilde{x}))$. The inequality is strict if J is strictly convex. In particular, looking at (45) and using $\Delta t < 1/(1 + \lambda)$, this implies that if $I^k(x) < I^k(\tilde{x})$, then $I^{k+1}(x) \leq I^{k+1}(\tilde{x})$. On the other hand we also have that if $I(x) = I(\tilde{x})$, then $\mathcal{H}_J(I(x)) = \mathcal{H}_J(I(\tilde{x}))$. Hence, if $I^k(x) = I^k(\tilde{x})$, then $I^{k+1}(x) = I^{k+1}(\tilde{x})$. This implies that the map from I^k to I^{k+1} transforms the level sets of I^k into level sets of I^{k+1} , and we can say that in the global case ($\omega = 1/\text{Area}(\mathbb{T})$) the algorithm does not destroy the topographic map structure of I_0 . In other terms, the family of level lines of I^k coincides with the family of level lines of I_0 for any iteration k . When *there is* a kernel $\omega(x, y)$ involved, this property is violated, but the violation is small in regions where I is smooth, and it may be locally unnoticeable. In case there is a discontinuity in I , the violation may be small depending on the

relative size of the kernel and the region where the discontinuity takes place. The proofs can be found in Appendix E.

In summary, our algorithm preserves locally the mutual relationship between image values but, at the same time, they can change at the global level. This novel formulation now complies with basic properties of visual perception (locality, eventual inversion of order in level lines).

C. A Further Connection With Neuroscience

We would like to mention a similarity between the equations that arise in the just proposed variational framework of ACE and the so-called Wilson–Cowan equations, that can be an interesting hint for further research. Let us remember that these last equations describe, according to [22]–[24], the temporal evolution of the activity of a population of neurons in the region $V1$ of the visual cortex.

Treating $V1$ as a planar sheet of nervous tissue, the state $a(r, \phi, t)$ of a population of cells with cortical space coordinates $r \in \mathbb{R}^2$ and orientation preference $\phi \in [0, \pi)$ can be modeled with the following PDE [24]

$$\frac{\partial a(r, \phi, t)}{\partial t} = -\alpha a(r, \phi, t) + \mu \int_0^\pi \int_{\mathbb{R}^2} \omega(r, \phi || r', \phi') \sigma(a(r', \phi', t)) dr' d\phi' + h(r, \phi, t) \quad (50)$$

where α, μ are coupling coefficients, $h(r, \phi, t)$ is the external input (visual stimuli), $\omega(r, \phi || r', \phi')$ is a kernel which decays with the differences $|r - r'|, |\phi - \phi'|$, σ is a sigmoid function and t is time. If we ignore the orientation ϕ and assume that the input h is constant in time, then we see that (50) shows a very similar structure as our gradient descent (45) in the particular case when $\tilde{\omega}(x, y) = \delta(x - y)$, where neural activity a plays the role of image value I , sigmoid function σ is our *slope function*, visual input h is our initial image I_0 . In fact, for this choice of $\tilde{\omega}$, which is the one used for our numerical implementation (see Section VIII), (45) becomes (44).

Finally, Cowan published a work [25] in which he links Retinex with the Wilson–Cowan equations. We are currently investigating these connections among Retinex, visual cortex activity models, and variational image processing.

VI. NUMERICAL APPROACH

Our numerical approach is based on the iterative scheme (45) which corresponds to an explicit discretization in time of (40). We want to point out several features of the scheme. For that, recall that we are assuming that we have normalized the initial image I_0 to take values in $[0, 1]$. Then its differences take values in $[-1, 1]$. As we shall prove below, this normalization condition will be preserved by the algorithm. On the other hand, the function s_α has been defined in (13), but it is not necessary to use exactly this form. In fact, since the slope function s_α is not differentiable at every point of its domain, to get good approximations it may be convenient to use instead a more smooth function, like a sigmoid type function. Let us denote by \tilde{s}_α the function we shall use in place of s_α , which may eventually coincide with it. The important features to be retained by \tilde{s}_α are its

oddness and its saturation at large values of the argument (both properties also hold for a sigmoid type function). In practice, we consider a smooth odd function $\tilde{s}(r)$ increasing from -1 (as $r \rightarrow -1$) to 1 (as $r \rightarrow 1$) and we define $\tilde{s}_\alpha(r) = \tilde{s}(\alpha r)$. For instance, we can use as $\tilde{s}(r)$ a rescaling of $\arctan(r)$. This is a sort of return to the original idea, in fact, a sigmoid type function has always been considered the most suitable also in the basic formulation of ACE, the slope function defined in (13) was preferred only because of computational reasons [5], [6].

Let us consider discrete images $I : \mathbb{T}_d \rightarrow [0, 1]$ as vectors in \mathbb{R}^{4WH} and denote by $\langle u, v \rangle$ (resp. $\|u\|, \|v\|$) the scalar product (resp. the norm) of two vectors and $u, v \in \mathbb{R}^{4WH}$. For any image $I : \mathbb{T}_d \rightarrow [0, 1]$, let us denote

$$\tilde{R}_I(x) := \sum_{y \in \mathbb{T}_d} \omega(x, y) \tilde{s}_\alpha(I(x) - I(y)) \quad (51)$$

and observe that $|\tilde{R}_I(x)| \leq 1$ for any $x \in \mathbb{T}_d$. Since we want perform estimations, we can consider here $M = 1$, which is certainly an upper bound for the values assumed by \tilde{R}_I . Then the numerical scheme (45) can be written as

$$I^{k+1}(x) = (1 - (1 + \lambda)\Delta t) I^k(x) + \Delta t \left(\frac{1}{2} + \frac{\tilde{R}_{I^k}(x)}{2} \right) + \Delta t \lambda I^0(x). \quad (52)$$

Thus, since I^0 takes values in $[0, 1]$, if I^k takes values in $[0, 1]$, then $|\tilde{R}_{I^k}(x)| \leq 1$ and

$$|I^{k+1}(x)| \leq 1 - (1 + \lambda)\Delta t + \Delta t + \Delta t \lambda = 1.$$

Thus, at any iteration $k \geq 0$, I^k takes values in $[0, 1]$. Since we are working in the discrete framework, this implies that there are convergent subsequences in $\{I^k\}_k$. This is a weak form of stability.

On the other hand, we have

$$E(I^{k+1}) \leq E(I^k) + C(\Delta t)^2 \quad (53)$$

for some constant $C > 0$. To prove this, we define $F(t) = E(I^k + t(I^{k+1} - I^k))$. Then, using the intermediate value theorem, there is a value $t^* \in (0, 1)$ for which $F(1) - F(0) = F'(t^*)$. Observe that, using (52), we have $\|I^{k+1} - I^k\| \leq 2(1 + \lambda)\Delta t \|\mathbf{1}\|$ (where $\mathbf{1}$ denotes the constant image equal to 1). Hence

$$\begin{aligned} E(I^{k+1}) - E(I^k) &= F'(t^*) \\ &= \langle \delta E(I^k + t^*(I^{k+1} - I^k)), (I^{k+1} - I^k) \rangle \\ &= \langle \delta E(I^k), (I^{k+1} - I^k) \rangle \\ &\quad + \langle \delta E(I^k + t^*(I^{k+1} - I^k)) - \delta E(I^k), (I^{k+1} - I^k) \rangle \\ &= -\Delta t \langle \delta E(I^k), \delta E(I^k) \rangle \\ &\quad + \langle \delta E(I^k + t^*(I^{k+1} - I^k)) - \delta E(I^k), (I^{k+1} - I^k) \rangle \\ &\leq -\Delta t \langle \delta E(I^k), \delta E(I^k) \rangle + C_0 \|I^{k+1} - I^k\|^2 \\ &\leq -\Delta t \langle \delta E(I^k), \delta E(I^k) \rangle + 4C_0(1 + \lambda)^2 (\Delta t)^2 \end{aligned}$$

where $C_0 > 0$ is a bound on the second derivative of E (which depends on a bound on the second derivative of \tilde{s}_α). Notice that (53) implies that

$$\frac{E(I^{k+1}) - E(I^k)}{\Delta t} \leq C\Delta t \quad (54)$$

and the right-hand side tends to zero as $\Delta t \rightarrow 0$, meaning that the derivative of the energy along the solution is negative. We conclude that our numerical scheme is stable (in the sense that it does not diverge) and decreases the energy up to an error of order $(\Delta t)^2$. We are not able to prove full convergence of the scheme (52) yet, but in all our experiments we reached a steady state in less than 60 iterations.

Remark 5: Using a fixed point argument we can easily prove the convergence of the numerical scheme (52) when $\lambda > \max_{r \in [-1,1]} |(d\tilde{s}_\alpha/dr)(r)| - 1$. This constraint implies a stronger attachment to data.

A. Speedup of the Algorithm

As we have mentioned earlier, one of the main problems with ACE is its computational cost. Indeed, the computational cost of ACE is the one given by of the sum

$$R_I(x) = \sum_{y \in \mathbb{T}_d} \omega(x, y) s_\alpha(I(x) - I(y)) \quad (55)$$

which is $\mathcal{O}(N)$, times the number N of pixels of the image. Thus, the complexity of ACE is $\mathcal{O}(N^2)$. This implies that with a standard PC (P4, 3 GHz) it will take from minutes to hours to process high resolution images. Now we show how to drastically speed up the process by taking the following numerical approximation. First, we approximate the function \tilde{s}_α by a polynomial (in a finite domain) which reduces the ACE computation to a finite number of convolutions. Then, we compute them using the fast Fourier transform (FFT), thus reducing the final complexity to $\mathcal{O}(N \log N)$, which, in practice, implies a computational time of just a few seconds per high resolution image.

Our first step consists in approximating \tilde{s}_α with a polynomial in the range $[-1, 1]$. For that, we fix the degree n and we look for the polynomial

$$\tilde{s}_\alpha^{(n)}(r) = \sum_{i=0}^n c_i r^i$$

which minimizes

$$\int_{-1}^1 (\tilde{s}_\alpha(r) - p(r))^2 dr$$

in the class of polynomials $p(r)$ of degree n . Observe that, being \tilde{s}_α an odd function, the solution of the above problem is also an odd polynomial. Again, we can look at this approximation in two different ways: either we consider it as an approximation to the result that would be obtained using \tilde{s}_α , or we just view it as another slope function.

Remark 6: Notice that, as $n \rightarrow +\infty$ the quadratic error between $\tilde{s}_\alpha^{(n)}$ and \tilde{s}_α goes to zero. However, in practice, we can get also a good approximation for the maximum error. For instance, taking $\alpha = 5$ and $n = 7$ we get a maximum error of 0.045 and

an average error of 0.021. In the scale of values $[0, 255]$, this amounts to an average error of 5.35. When $\alpha = 5$ and $n = 9$ the average error is 0.012, and so on. In other words, increasing the degree of the approximating polynomial we increase the accuracy of our result, but even with relatively small degrees the approximations are often visually indistinguishable from the ones obtained with ACE (using the original function \tilde{s}_α).

Mathematically, a better estimation of the error and a better approximation can be obtained by using the Chebyshev approximation to \tilde{s}_α which is an approximation to the minimax polynomial (this polynomial provides the best approximation in the maximum norm, see [18]), a method that is being implemented at present. Observe that the solution of (27) with $J' = \tilde{s}_\alpha^{(n)}$ is an approximate solution of (27) with $J' = \tilde{s}_\alpha$ since the replacement of one function by the other results in a correction term or error bounded by $\max_{r \in [-1,1]} |\tilde{s}_\alpha(r) - \tilde{s}_\alpha^{(n)}(r)|$.

Now we are able to show how, using $\tilde{s}_\alpha^{(n)}$, we can drastically reduce the computational complexity. Let us evaluate $\tilde{s}_\alpha^{(n)}(I(x) - I(y))$

$$\begin{aligned} & \tilde{s}_\alpha^{(n)}(I(x) - I(y)) \\ &= -\tilde{s}_\alpha^{(n)}(I(y) - I(x)) \\ &= -\sum_{i=0}^n c_i (I(y) - I(x))^i \\ &= -\sum_{i=0}^n c_i \sum_{j=0}^i \binom{i}{j} I(y)^j (-I(x))^{i-j} \\ &= \sum_{j=0}^n \left[\sum_{i=0}^j (-1)^{i-j+1} c_i \binom{i}{j} I(x)^{i-j} \right] I(y)^j \quad (56) \end{aligned}$$

where $\binom{i}{j} = i!/(j!(i-j)!)$.

The quantity between square brackets depends only on $I(x)$ and on the coefficients c_i , this implies that $\tilde{s}_\alpha^{(n)}(I(x) - I(y))$ can be simply written as a polynomial of order n in the variable $I(y)$

$$\tilde{s}_\alpha^{(n)}(I(x) - I(y)) = \sum_{i=0}^n a_i I(y)^i \quad (57)$$

where the coefficients a_i given by the sum in square brackets in (56), $i = 1, \dots, n$, do not depend on $I(y)$, but only on $I(x)$ and on \tilde{s}_α . Now, if we replace $s_\alpha(I(x) - I(y))$ in (55) by $\tilde{s}_\alpha^{(n)}(I(x) - I(y))$, we get an approximation of $R(x)$ at order n of the form

$$\tilde{R}^{(n)}(x) := \sum_{i=0}^n a_i \sum_{y \in \mathbb{T}_d} I(y)^i \omega(x, y). \quad (58)$$

The great advantage of this approximation is that the dependence on $I(x)$ is confined in the n coefficients a_i , whose computation complexity is $\mathcal{O}(1)$. Being $\omega(x, y)$ a function of $x - y$, the inner sums in (58) are convolutions which can be precomputed (for all the input image pixels) using the FFT with a complexity $\mathcal{O}(N \log N)$.

In conclusion, we have shown that considering the approximated version $\tilde{R}^{(n)}(x)$, instead of $R(x)$, yields to a computational complexity for ACE of $\mathcal{O}(N \log N)$. In practice, this means that we can process one iteration of ACE on a 400×270

image in about 1 s on a standard PC (P4, 3 GHz), instead of tens of minutes with the original procedure.

VII. TUNING THE ALGORITHM

The variational formulation of ACE keeps the original parameters in a slightly different implementation. Let us recall the basic ACE parameters [5], [6] and briefly comment on their variational version.

The original slope function is kept as it is, implemented with numerical approximation exposed above. Its meaning and effect remain unchanged. Changing the slope of the function tunes the final contrast: the bigger the slope, the greater the contrast.

The other basic parameter in the original ACE formulation is the shape of the weighting kernel ω . As in the basic ACE, the shape of the kernel and its *width* are responsible for the weight of mutual chromatic influence between pixels. A visual example of the shape of the filter locality can be seen in Fig. 5, where the input image on the left is filtered with two different kernels, the first isotropic (middle) and the second anisotropic (right). As well as in its basic formulation, choosing the kernel shape is the way to control the local effect of the image correction.

In later versions of ACE [26], two parameters have been added: Keep Original Grey (KOG) and Keep Original Dynamic Range (KODR). KOG retains the original mean image value and KODR its original dynamic range. These are conservative features that prevent the algorithm to over-filter images that a user would want to keep closer to the original. For instance, this is the case for low-key and high-key images like the fade-in and fade-out frames in movie transitions.

KOG is devised to relax the global GW mechanism. Instead of centering the chromatic channels around the medium gray, the “keep original gray” function preserves the original mean values (independently in the three chromatic channels). This results in histograms more similar in shape with the original. This function is implemented in the variational formulation in the attachment term of (45). Regarding KODR, sometimes the use of a limited dynamic range allows us to obtain specific visual effects. If necessary, this can be preserved changing the final normalization stage in both versions of ACE.

Both parameters are implemented in the variational formulation using the attachment to data technique.

VIII. EXPERIMENTS

Recall that our numerical scheme is given by (52). Our choice of parameters has been the same (unless otherwise specified) for all the experiments shown in this section. So although these parameters should be tuned for specific applications, we have found overall good results with the following set: $\Delta t = 0.15$, $\lambda = 1$, a polynomial approximation of \tilde{s}_α of degree $n = 7$, a slope function with $\alpha = 10$ and a kernel ω of Gaussian shape. We have tested our algorithm using a nonoptimized C++ implementation running on a P4, 3-GHz Linux machine. Typically, for a 400×270 image, we achieve the steady state (less than 0.5% of RMS difference from one iteration to the next) after 25–30 iterations, with a total processing time of 25–30 s. Since we are running an explicit iterative scheme implementing a PDE, a great increase in speed could be obtained by programming the algorithm directly on a Graphics Card [27].

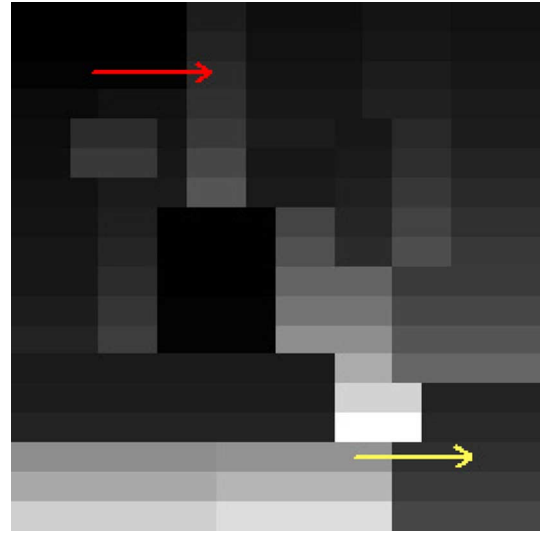


Fig. 3. Land and McCann’s black and white Mondrian experiment [15], [16]. The rectangle marked with the top arrow has a lower grey value than the rectangle marked with the bottom arrow, but it is perceived as being lighter.

Let us start by remarking the importance of the local behavior of our algorithm. Fig. 4 shows a greyscale image (top left) and the results of applying global equalization (top middle) and our algorithm (top right). Notice how our algorithm performs a local modification of gray values according to their distance from the edges, following qualitatively the HVS perceptual response. This does not come out using a global equalization technique, as the same figure shows (see also the corresponding scan lines in the bottom line).

In Fig. 5, we see how the shape of the weighting kernel ω can affect the final result. In the middle image of this figure ω is rotationally invariant, while in the image on the right the kernel is elongated in the vertical direction.

Fig. 6 shows the application of our algorithm to the de-quantization of images. On the top left, we have the original image, encoded in 8 bits, 256 colors. The bottom left the red channel histogram shows typical disjoint spikes, while on the right re-computed intermediate values are visible, running through the whole 24 bits palette.

Fig. 7 shows the application of our algorithm to film restoration [26], [28], [29]. In this example, a frame from an old 8-mm film positive shows a very strong red cast. This red cast is mostly removed by our technique: the colors now look natural and new ones appear.

Fig. 8 shows the effect of the slope in the final results. On the left, we have the original image, in the middle the result obtained by our algorithm with a slope function $\alpha = 10$, on the right with the signum function (corresponding to a slope $\alpha = \infty$). We can see that, by increasing the slope, we increase the contrast, and we obtain very saturated colors; however, some information is lost (e.g., the window reflections on the wall).

Finally, Fig. 9 shows the local effect of our algorithm on the color enhancement of a typical back-light sunset landscape. Notice that, while the sky color and brightness are visually preserved, details in the shadow below the car are enhanced.

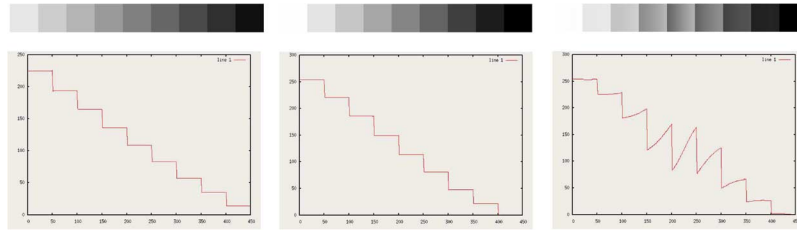


Fig. 4. Top row: (left) original grayscale image, (middle) enhanced with global histogram equalization, and (right) enhanced with proposed algorithm. Bottom row: corresponding profiles of scan lines.

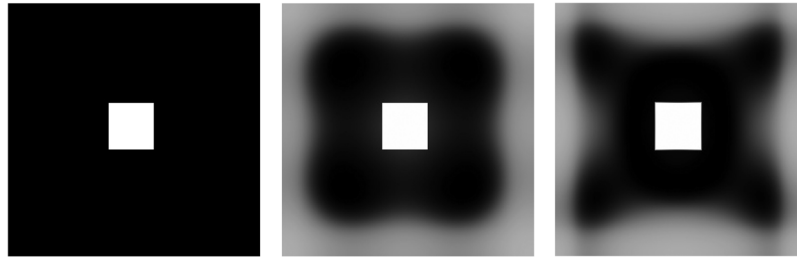


Fig. 5. (Left) Original image, (middle) filtered using isotropic kernel, and (right) filtered using anisotropic kernel.

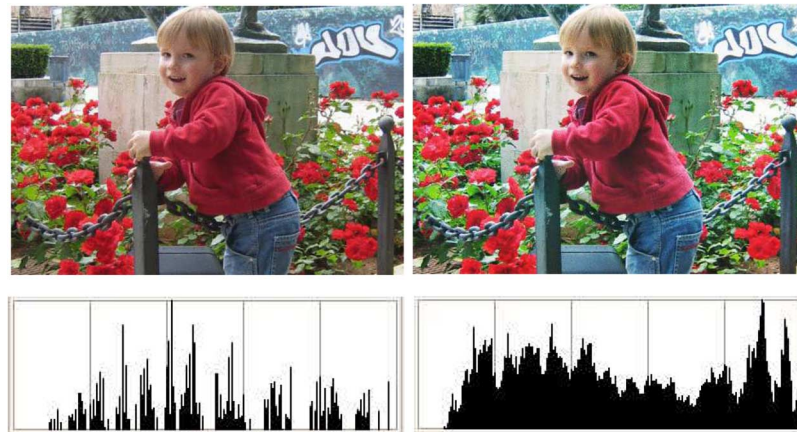


Fig. 6. (Top left) Original image, (top right) color enhanced, (bottom left) original red channel histogram, and (bottom right) color enhanced image red channel histogram.

IX. CONCLUSION AND FUTURE WORK

In this paper, we have investigated global and local properties of color correction algorithms from the viewpoint of variational techniques. In particular, we focused our attention on the variational formulation of ACE, a color correction model that takes into account some of the most important features of human color perception. The variational formulation of ACE allowed us to clarify its global and local characteristics, which were somewhat hidden in its basic formulation [5], [6]. Furthermore, the approximation of the continuous variational formulation of ACE using a polynomial approximation leads to a significant reduction of the corresponding algorithm complexity, decreasing from $\mathcal{O}(N^2)$ to $\mathcal{O}(N \log N)$ without introducing significant changes in the results. This allows a very fast implementation. Several subjects remain to be investigated: the effects of the kernel function ω on local behavior, the variational formulation of other color perception algorithms like Retinex and the connection with the Wilson–Cowan equations for neuronal activity in the visual cortex.

APPENDIX

A. Proof of Equation (2)

Let $\psi : [0, 1] \rightarrow \mathbb{R}$ be a differentiable function defined in the codomain of the image function. Consider the functional

$$E(I) = \int_{\mathcal{I}} \psi(I(x)) dx - \frac{1}{WH} \int_{\mathcal{I}} \int_{\mathcal{I}} |I(x) - I(y)| dx dy. \quad (59)$$

Let us prove that the first variation of the energy $E(I)$ is given by

$$\delta E(I) = \psi'(I(x)) + 2 - \frac{4}{WH} \int_{\mathcal{I}} \text{sign}^+(I(x) - I(y)) dy \quad (60)$$

where

$$\text{sign}^+(t) = \begin{cases} 1, & t > 0 \\ \frac{1}{2}, & t = 0 \\ 0, & t < 0 \end{cases}.$$



Fig. 7. (Left) Original image; (right) color enhanced. Original image courtesy A. Pardo.



Fig. 8. (Left) Original image, (middle) color enhanced with slope function, and (right) color enhanced with sign function. Courtesy of P. Greenspun.



Fig. 9. (Left) Original image; (right) color enhanced. Courtesy of P. Greenspun.

Since the absolute value is not differentiable at 0, let us approximate it by the differentiable function

$$|z|_\epsilon := \sqrt{\epsilon^2 + |z|^2} \quad z \in \mathbb{R}, \epsilon > 0 \quad (61)$$

whose derivative is

$$\text{sign}_\epsilon(z) = \frac{z}{\sqrt{\epsilon^2 + |z|^2}} \quad z \in \mathbb{R}. \quad (62)$$

Let

$$E_\epsilon(I) = \int_{\mathcal{J}} \psi(I(x)) dx - \frac{1}{WH} \int_{\mathcal{J}^2} |I(x) - I(y)|_\epsilon dx dy. \quad (63)$$

Denoting δI the perturbation of I , the computation of its variation gives

$$\begin{aligned} \delta E_\epsilon(I, \delta I) &= \int_{\mathcal{J}} \psi'(I(x)) \delta I(x) dx \\ &\quad - \frac{1}{WH} \int_{\mathcal{J}^2} \text{sign}_\epsilon(I(x) - I(y)) (\delta I(x) - \delta I(y)) dx dy \end{aligned} \quad (64)$$

where we have denoted $\partial \psi / \partial I|_{I(x)}$ with $\psi'(I(x))$ for simplicity. The last term in the previous equation can be decomposed as

$$\begin{aligned} &\int_{\mathcal{J}^2} \text{sign}_\epsilon(I(x) - I(y)) \delta I(x) dx dy \\ &\quad - \int_{\mathcal{J}^2} \text{sign}_\epsilon(I(x) - I(y)) \delta I(y) dx dy. \end{aligned} \quad (65)$$

Since $\text{sign}_\epsilon(I(y) - I(x)) = -\text{sign}_\epsilon(I(x) - I(y))$, interchanging the role of x and y in the second integral we get

$$\begin{aligned} &\int_{\mathcal{J}^2} \text{sign}_\epsilon(I(x) - I(y)) (\delta I(x) - \delta I(y)) dx dy \\ &= 2 \int_{\mathcal{J}^2} \text{sign}_\epsilon(I(x) - I(y)) \delta I(x) dx dy. \end{aligned} \quad (66)$$

Thus, we have

$$\delta E_\epsilon(I, \delta I) = \int_{\mathbb{T}} \left(\psi'(I(x)) - \frac{2}{WH} \times \int_{\mathbb{T}} \text{sign}_\epsilon(I(x) - I(y)) dy \right) \delta I(x) dx \quad (67)$$

and the first variation of E_ϵ at I is

$$\delta E_\epsilon(I) = \psi'(I(x)) - \frac{2}{WH} \int_{\mathbb{T}} \text{sign}_\epsilon(I(x) - I(y)) dy. \quad (68)$$

Letting $\epsilon \rightarrow 0_+$, we obtain

$$\delta E(I) = \psi'(I(x)) - \frac{2}{WH} \int_{\mathbb{T}} \text{sign}_0(I(x) - I(y)) dy \quad (69)$$

where

$$\text{sign}_0(t) = \begin{cases} 1, & t > 0 \\ 0, & t = 0 \\ -1, & t < 0 \end{cases}$$

Since $\text{sign}_0(t) = 2\text{sign}^+(t) - 1$, the right-hand side of (69) becomes (2).

B. Proof of Remark 1

Proposition 1 can be extended for any convex even function J , even if it is not differentiable. In fact, recall that, if Ψ is a convex function defined in a Hilbert space \mathcal{H} , then its subdifferential at I is the set of subtangents $\partial\Psi(I) \subset \mathcal{H}$, that is, $F \in \partial\Psi(I)$ if

$$\Psi(\tilde{I}) - \Psi(I) \geq \langle F, \tilde{I} - I \rangle \quad \forall \tilde{I} \in \mathcal{H} \quad (70)$$

being $\langle \cdot, \cdot \rangle$ the inner product carried by \mathcal{H} . The analogous statement of Proposition 1 says that the subdifferential of $C_{\omega, J}$ (defined in $L^2(\mathbb{T})$, the Hilbert space of square integrable functions on \mathbb{T}) at I consists of the functions which can be written in the form

$$2 \int_{\mathbb{T}} \omega(x, y) g(x, y) dy \quad (71)$$

where $g(x, y) \in \partial J(I(y) - I(x))$ for almost any point $(x, y) \in \mathbb{T} \times \mathbb{T}$. A particular instance of this situation is the case where $J(r) = |r|$; in that case, we have

$$\delta C_{\omega, J}(I) := 2 \int_{\mathbb{T}} \omega(x, y) g(x, y) dy \quad (72)$$

where $g(x, y)$ is a selection of $\text{sign}(I(y) - I(x))$, that is $g(x, y) = +1$ if $I(y) - I(x) > 0$, $g(x, y) = -1$ if $I(y) - I(x) < 0$ and $g(x, y) \in [-1, 1]$ if $I(y) - I(x) = 0$.

C. Proof of Proposition 2

Since

$$\delta D_{\tilde{\omega}, I_0}(I)(\delta I) = \lim_{t \rightarrow 0^+} \frac{1}{t} (D_{\tilde{\omega}, I_0}(I + t\delta I) - D_{\tilde{\omega}, I_0}(I)) \quad (73)$$

we have

$$\delta D_{\tilde{\omega}, I_0}(I)(\delta I) = 2 \int_{\mathbb{T}^2} \tilde{\omega}(x, y) (I(y) - \tilde{I}^{\tilde{\omega}}(x)) \delta I(y) dx dy.$$

Since

$$\begin{aligned} \int_{\mathbb{T}^2} \tilde{\omega}(x, y) I(y) \delta I(y) dx dy &= \int_{\mathbb{T}} I(y) \delta I(y) \int_{\mathbb{T}} \tilde{\omega}(x, y) dx dy \\ &= \int_{\mathbb{T}} I(y) \delta I(y) dy \end{aligned} \quad (74)$$

and

$$\begin{aligned} \int_{\mathbb{T}^2} \tilde{\omega}(x, y) \tilde{I}^{\tilde{\omega}}(x) \delta I(y) dx dy \\ = \int_{\mathbb{T}} \left(\int_{\mathbb{T}} \tilde{\omega}(x, y) \tilde{I}^{\tilde{\omega}}(x) dx \right) \delta I(y) dy \end{aligned}$$

we obtain (26). \square

D. Proof of Remark 2

In the case that J is any convex function and I^* is a minimum of $E_{\tilde{\omega}, \omega}(I)$, using the definition of subdifferential introduced in the proof of Remark 1, Section B, we have

$$\begin{aligned} 0 &\leq E_{\tilde{\omega}, \omega}(I) - E_{\tilde{\omega}, \omega}(I^*) \\ &\leq D_{\tilde{\omega}}(I) - D_{\tilde{\omega}}(I^*) + \langle \delta C_{\omega, J}(I^*), I^* - I \rangle \end{aligned}$$

where $\langle \cdot, \cdot \rangle$ here denotes the scalar product in $L^2(\mathbb{T})$. Letting $I = I^* + t\delta I$, $t > 0$, we have

$$0 \leq t\delta D_{\tilde{\omega}}(I^*, \delta I) + o(t) + t \langle \delta C_{\omega, J}(I^*), \delta I \rangle$$

where $o(t)/t \rightarrow 0$ as $t \rightarrow 0^+$. Dividing by t and letting $t \rightarrow 0^+$, we obtain

$$0 \leq \delta D_{\tilde{\omega}}(I^*, \delta I) - \langle \delta C_{\omega, J}(I^*), \delta I \rangle \quad (75)$$

for any perturbation δI . This implies that

$$\delta D_{\tilde{\omega}}(I^*) - \delta C_{\omega, J}(I^*) = 0. \quad (76)$$

This remark permits to have the analogous of Proposition 1 when $J(r) = |r|$.

E. Proof of Proposition 4

Let us write again the statement of Proposition 4.

Let $J : \mathbb{R} \rightarrow [0, \infty)$ be a convex function. Let us consider the operator

$$\mathcal{H}_J(I(x)) = \int_{\mathbb{T}} J'(I(x) - I(y)) dy. \quad (77)$$

Then

$$(\mathcal{H}_J(I(x)) - \mathcal{H}_J(I(\tilde{x}))) \cdot (I(x) - I(\tilde{x})) \geq 0. \quad (78)$$

Let us first include the proof and then discuss its meaning.

Proof: Observe

$$\begin{aligned} & (\mathcal{H}_J(I)(x) - \mathcal{H}_J(I)(\tilde{x})) \cdot (I(x) - I(\tilde{x})) \\ &= \int_{\mathbb{T}} (J'(I(x) - I(y)) - J'(I(\tilde{x}) - I(y))) \cdot (I(x) - I(\tilde{x})) dy. \end{aligned}$$

The convexity of J implies

$$(J'(I(x) - I(y)) - J'(I(\tilde{x}) - I(y))) \cdot (I(x) - I(\tilde{x})) \geq 0 \quad (79)$$

and our statement follows. \square

We have already given the interpretation of Proposition 4 in Section V-B. We have explained that in the case that $\omega = 1$, then each iteration of our algorithm (45) respects the family of level sets of the image (we refer to this as the preservation of the topographic structure of the image). Is this true in the local case, when there is a kernel $\omega(x, y)$ involved? The preservation of the topographic map structure of I_0 is not guaranteed in the case of local contrast enhancement and there can be an intertwining between image values. This is desirable for the reproduction of some perceptual behavior of the HVS, e.g., Land's experiment shown in Fig. 3. On the other hand, the intertwining may not be noticeable locally. To explain this, again we analyze the effect of the operator $\mathcal{H}_{\omega, J}$. Let us observe that if the image $I : \mathbb{T} \rightarrow [0, M]$ is continuous at pixel $x \in \mathbb{T}$ and the function J' is continuous, then $\mathcal{H}_{\omega, J}(I)$ is also continuous at x , and this amounts to say that the gray level difference between $\mathcal{H}_{\omega, J}(I)(x)$ and $\mathcal{H}_{\omega, J}(I)(\tilde{x})$ for \tilde{x} near x is small. It is also interesting to compute $\mathcal{H}_{\omega, J}(I)$ when I is a pure edge given by $I(y) = 1$ if $y = (y_1, y_2)$ and $y_1 \geq 0$ and $I(y) = 0$ if $y_1 < 0$. In that case, being $x = (x_1, x_2)$

$$\begin{aligned} \mathcal{H}_{\omega, J}(I)(x) &= \frac{J'(-1)}{2}, \quad \text{if } x_1 < 0 \quad \text{and} \\ \mathcal{H}_{\omega, J}(I)(x) &= \frac{J'(1)}{2}, \quad \text{if } x_1 \geq 0. \end{aligned}$$

Thus, in this case, (78) holds. This only indicates that for edges where the localization error is small, the violation of the order of level lines may be locally unnoticeable. However, as we mentioned in Section V-B, this is compatible with a change in the order of image values at the global level complying with basic properties of visual perception.

The same computations can be done for color images but the interpretation is more complex. In that case, we just observe that if $\vec{I} : \mathbb{T} \rightarrow [0, 1]^3$, $J : \mathbb{R}^3 \rightarrow [0, \infty)$ is a convex function, and we define

$$\mathcal{H}_J(\vec{I}(x)) = \int_{\mathbb{T}} \nabla J(\vec{I}(x) - \vec{I}(y)) dy \quad (80)$$

then $\mathcal{H}_J(\vec{I}(x)) = \mathcal{H}_J(\vec{I}(\tilde{x}))$ if $I(x) = I(\tilde{x})$. It follows that points with the same color will *locally* have the same color after a transformation with \mathcal{H}_J .

F. Proof of Proposition 3

For simplicity of notation, let us fix the proof on the case where $D_{\tilde{\omega}}^d(I) = D_{\tilde{\omega}, I_0}^d(I)$ [see (31)], the proof being identical

in the general case (22). First, we prove that

$$\inf_I E_{\tilde{\omega}, \omega}^d > -\infty. \quad (81)$$

To this aim, we observe

$$\begin{aligned} D_{\tilde{\omega}}^d(I) &= \sum_{x \in \mathbb{T}_d} I(x)^2 + \sum_{x \in \mathbb{T}_d} \tilde{T}^{\tilde{\omega}}(x)^2 \\ &\quad - 2 \sum_{x \in \mathbb{T}_d} \sum_{y \in \mathbb{T}_d} \tilde{\omega}(x, y) I(y) \tilde{T}^{\tilde{\omega}}(x). \end{aligned} \quad (82)$$

On the other hand, using our assumptions on J , we have

$$C_{\omega, J}^d(I) \leq 2C \sum_{x \in \mathbb{T}_d} |I(x)|. \quad (83)$$

Using the Cauchy–Schwartz inequality, the inequality $ab \leq \epsilon(a^2/2) + (b^2/2\epsilon)$, $a, b, \epsilon > 0$, and fixing $\epsilon = 1/2C$, we may write

$$\begin{aligned} \sum_{x \in \mathbb{T}_d} |I(x)| &\leq \sqrt{4WH} \left(\sum_{x \in \mathbb{T}_d} |I(x)|^2 \right)^{1/2} \\ &\leq \frac{1}{4C} \sum_{x \in \mathbb{T}_d} |I(x)|^2 + 4CWH. \end{aligned} \quad (84)$$

Hence

$$C_{\omega, J}^d(I) \leq \frac{1}{2} \sum_{x \in \mathbb{T}_d} |I(x)|^2 + 8C^2WH. \quad (85)$$

We deduce that

$$\begin{aligned} E_{\tilde{\omega}, \omega}^d(I) &= D_{\tilde{\omega}}^d(I) - C_{\omega, J}^d(I) \\ &\geq \frac{1}{2} \sum_{x \in \mathbb{T}_d} |I(x)|^2 + \sum_{x \in \mathbb{T}_d} \tilde{T}^{\tilde{\omega}}(x)^2 \\ &\quad - 2 \sum_{x \in \mathbb{T}_d} \sum_{y \in \mathbb{T}_d} \tilde{\omega}(x, y) I(y) \tilde{T}^{\tilde{\omega}}(x) - 8C^2WH. \end{aligned}$$

Now, using again the inequality $ab \leq \epsilon(a^2/2) + (b^2/2\epsilon)$ with $\epsilon = 1/4$ and the convexity of the square function, we have

$$\begin{aligned} & \sum_{x \in \mathbb{T}_d} \sum_{y \in \mathbb{T}_d} \tilde{\omega}(x, y) I(y) \tilde{T}^{\tilde{\omega}}(x) \\ & \leq \left(\sum_{x \in \mathbb{T}_d} \left(\sum_{y \in \mathbb{T}_d} \tilde{\omega}(x, y) I(y) \right)^2 \right)^{1/2} \left(\sum_{x \in \mathbb{T}_d} \tilde{T}^{\tilde{\omega}}(x)^2 \right)^{1/2} \\ & \leq \frac{1}{8} \sum_{x \in \mathbb{T}_d} \left(\sum_{y \in \mathbb{T}_d} \tilde{\omega}(x, y) I(y) \right)^2 + 2 \sum_{x \in \mathbb{T}_d} \tilde{T}^{\tilde{\omega}}(x)^2 \\ & \leq \frac{1}{8} \sum_{x \in \mathbb{T}_d} \sum_{y \in \mathbb{T}_d} \tilde{\omega}(x, y) I(y)^2 + 2 \sum_{x \in \mathbb{T}_d} \tilde{T}^{\tilde{\omega}}(x)^2 \\ & \leq \frac{1}{8} \sum_{y \in \mathbb{T}_d} I(y)^2 + 2 \sum_{x \in \mathbb{T}_d} \tilde{T}^{\tilde{\omega}}(x)^2. \end{aligned}$$

Combining the last two inequalities, we obtain

$$E_{\tilde{\omega}, \omega}^d(I) \geq \frac{1}{4} \sum_{x \in \mathbb{T}_d} |I(x)|^2 - 3 \sum_{x \in \mathbb{T}_d} \tilde{T}^{\tilde{\omega}}(x)^2 - 8C^2WH$$

and (81) follows. Now, if I_k is a minimizing sequence for $E_{\tilde{\omega},\omega}^d$, i.e., $E_{\tilde{\omega},\omega}^d(I_k) \rightarrow \inf_I E_{\tilde{\omega},\omega}^d(I)$, from the last computations, we have

$$\frac{1}{4} \sum_{x \in \mathbb{T}_d} |I_k(x)|^2 \leq E_{\tilde{\omega},\omega}^d(I_k) + 3 \sum_{x \in \mathbb{T}_d} \tilde{T}^{\tilde{\omega}}(x)^2 + 8C^2WH \quad (86)$$

and we deduce that I_k is bounded in \mathbb{R}^{4WH} . Thus, there is a subsequence of I_k , which we denote again by I_k , and an image $I^* : \mathbb{T}_d \rightarrow [0, 1]$ such that $I_k \rightarrow I^*$. Then $E_{\tilde{\omega},\omega}^d(I_k) \rightarrow E_{\tilde{\omega},\omega}^d(I^*)$ and we deduce that I^* is a minimum of $E_{\tilde{\omega},\omega}^d$. \square

G. Proof of Remark 3

The fact that the energy is bounded from below, i.e., inequality (81), can be proved with the analogous proof in the continuous case. What is missing in the continuous case is the fact that bounded sequences in the Hilbert space $L^2(\mathbb{T})$ of square integrable functions in \mathbb{T} converge in the norm of $L^2(\mathbb{T})$, a fact which is necessary to pass to the limit to guarantee that

$$E_{\tilde{\omega},\omega}^d(I_k) \rightarrow E_{\tilde{\omega},\omega}^d(I^*) \quad (87)$$

in the above proof. Observe that we only have that bounded sequences in $L^2(\mathbb{T})$ converge weakly. This would imply that $C_{\omega,J}(G * I_k) \rightarrow C_{\omega,J}(G * I^*)$ if we use a regularized version of the contrast

$$C_{\omega,J}(G * I) := \int_{\mathbb{T}} \int_{\mathbb{T}} \omega(x,y) J(G * I(x) - G * I(y)) dx dy \quad (88)$$

where G is some regularization kernel that maps weakly convergent to norm convergent sequences (like a Gaussian kernel). On the other hand, it implies also that $D_{\tilde{\omega}}(I^*) \leq \liminf_k D_{\tilde{\omega}}(I_k)$. Both things together imply that $E_{\tilde{\omega},\omega}^d(I^*) \leq \liminf_k E_{\tilde{\omega},\omega}^d(I_k)$; hence, $E_{\tilde{\omega},\omega}^d(I^*) = \inf_I E_{\tilde{\omega},\omega}^d(I)$ and the analogous assertion to (87) holds.

REFERENCES

- [1] G. Sapiro and V. Caselles, "Histogram modification via differential equations," *J. Diff. Eq.*, vol. 135, no. 2, pp. 238–266, 1997.
- [2] V. Caselles, J. M. Morel, G. Sapiro, and A. Tannenbaum, "Introduction to the special issue on partial differential equations and geometry driven diffusion in image processing and analysis," *IEEE Trans. Image Process.*, vol. 7, no. 3, pp. 269–273, Mar. 1998.
- [3] G. Sapiro, *Geometric Partial Differential Equations and Image Analysis*. Cambridge, U.K.: Cambridge Univ. Press, 2001, 0-521-79075-1.
- [4] R. Kimmel, M. Elad, D. Shaked, R. Keshet, and I. Sobel, "A variational framework for Retinex," *Int. J. Comput. Vis.*, vol. 52, no. 1, pp. 7–23, 2003.
- [5] A. Rizzi, C. Gatta, and D. Marini, "A new algorithm for unsupervised global and local color correction," *Pattern Recognit. Lett.*, vol. 124, pp. 1663–1677, 2003.
- [6] —, "From Retinex to automatic color equalization: Issues in developing a new algorithm for unsupervised color equalization," *J. Electron. Imag.*, vol. 13, no. 1, pp. 75–84, Jan. 2004.
- [7] E. Land, "An alternative technique for the computation of the designator in the Retinex theory of color vision," *Proc. Nat. Acad. Sci. USA*, vol. 83, pp. 3078–3080, 1986.
- [8] —, "Recent advances in Retinex theory and some implications for cortical computations: Color vision and the natural image," *Proc. Nat. Acad. Sci. USA*, vol. 80, pp. 5163–5169, 1983.
- [9] R. C. Gonzales and R. E. Woods, *Digital Image Processing*, 2nd ed. Englewood Cliffs, NJ: Prentice-Hall, 2002.
- [10] J. J. McCann and A. V., "Special session on Retinex at 40," *J. Electron. Imag.*, vol. 13, no. 1, pp. 6–145, 2004.
- [11] G. Buxbaum, "A spatial processor model for object color perception," *J. Franklin Inst.*, vol. 310, no. 1, p. 126, 1980.

- [12] O. Creutzfeld, B. Lange-Malecki, and K. Wortmann, "Darkness induction, Retinex and cooperative mechanisms in vision," *Exp. Brain Res.*, vol. 67, pp. 270–283, 1987.
- [13] O. Creutzfeld, B. Lange-Malecki, and E. Dreyer, "Chromatic induction and brightness contrast: A relativistic color model," *J. Opt. Soc. Amer. A*, vol. 7, no. 9, pp. 1644–1653, 1990.
- [14] L. M. Hurvich and D. Jameson, "Theory of brightness and color contrast in human vision," *Vis. Res.*, vol. 4, pp. 135–154, 1990.
- [15] E. Land and J. J. McCann, "Lightness and Retinex theory," *J. Opt. Soc. Amer. A*, vol. 61, pp. 1–11, 1977.
- [16] E. Land, "The Retinex theory of color vision," *Sci. Amer.*, vol. 237, no. 3, pp. 2–17, 1977.
- [17] J. J. McCann, "The role of simple nonlinear operations in modelling human lightness and color sensation," *Proc. SPIE*, vol. 1077, 1989.
- [18] W. T. Wetterling, B. P. Flannery, W. H. Press, and S. A. Teukolsky, *Numerical Recipes in C: The Art of Scientific Computing*. Cambridge, U.K.: Cambridge Univ. Press, 2002.
- [19] E. Provenzi, L. De Carli, A. Rizzi, and D. Marini, "Mathematical definition and analysis of the Retinex algorithm," *J. Opt. Soc. Amer. A*, vol. 22, pp. 2613–2621, 2005.
- [20] J. Serra, *Image Analysis and Mathematical Morphology*. New York: Academic, 1982.
- [21] V. Caselles, B. Coll, and J. M. Morel, "Topographic maps and local contrast changes in natural images," *Int. J. Comput. Vis.*, vol. 33, pp. 5–27, 1999.
- [22] H. R. Wilson and J. D. Cowan, "Excitatory and inhibitory interactions in localized populations of model neurons," *Biophys. J.*, vol. 12, pp. 1–24, 1972.
- [23] —, "A mathematical theory of the functional dynamics of cortical and thalamic nervous tissue," *Kybernetik*, vol. 13, pp. 55–80, 1973.
- [24] P. C. Bressloff, J. D. Cowan, M. Golubitsky, P. J. Thomas, and M. C. Wiener, "Geometric visual hallucinations, Euclidean symmetry and the functional architecture of striate cortex," *Phil. Trans. Roy. Soc. Lond. B*, vol. 356, pp. 299–330, 2001.
- [25] J. D. Cowan and P. C. Bressloff, "Visual cortex and the Retinex algorithm," presented at the SPIE Electronic Imaging Conf., San Jose, CA, 2002.
- [26] A. Rizzi, C. Gatta, C. Slanzi, G. Ciocca, and R. Schettini, "Unsupervised color film restoration using adaptive color equalization," *Lecture Notes Comput. Sci.*, vol. 3736, pp. 1–12, Dec. 2006.
- [27] M. Bertalmio, P. Fort, and D. Sánchez-Crespo, "Real-time, accurate depth of field using anisotropic diffusion and programmable graphics cards," in *Proc. 2nd Int. Symp. 3D Data Processing, Visualization and Transmission*, Sep. 6–9, 2004, pp. 767–773.
- [28] M. Chambah, C. Saint-Jean, F. Helt, and A. Rizzi, "Further image quality assessment in digital film restoration," presented at the IS&T/SPIE Electronic Imaging Conf., San José, CA, Jan. 2006.
- [29] A. Rizzi, "Perceptual colour film restoration," in *Proc. 3rd Int. Conf. Preservation and Conservation Issues Related to Digital Printing and Digital Photography*, London, U.K., Apr. 2006, pp. 24–25.

Marcelo Bertalmio received the B.Sc. and M.Sc. degrees from the Universidad de la Republica, Uruguay, in 1996 and 1998, respectively, and the Ph.D. degree from the University of Minnesota, Minneapolis, in 2001.

He is an Associate Professor at the Universitat Pompeu Fabra, Barcelona, Spain.

Vicent Caselles (A'94) received the Licenciatura and Ph.D. degrees in mathematics from Valencia University, Spain, in 1982 and 1985, respectively.

Currently, he is a Professor at the Universitat Pompeu Fabra, Barcelona, Spain. His research interests include image processing, computer vision, and the applications of geometry and partial differential equations to both fields.

Edoardo Provenzi received the degree in physics from the Università di Milano, Milano, Italy, in 2000, and the Ph.D. degree in mathematics and applications from the University of Genova, Italy, in 2003.

He is currently a Researcher with the Dipartimento di Tecnologia dell'Informazione, Università di Milano, where he works in the field of mathematical models of color vision and imaging.

Alessandro Rizzi received the degree in computer science from the Università di Milano, Milano, Italy, and the Ph.D. degree in information engineering from the Università di Brescia, Brescia, Italy.

He is currently an Assistant Professor with the Dipartimento di Tecnologia dell'Informazione, Università di Milano, where he teaches multimedia and human-computer interaction. Since 1990, he has been doing research in the field of digital imaging and vision. His main research topic is the use of color information in computer vision with particular attention to color perception mechanisms. He is the Coordinator of the Italian Color Group.